Conformation-dependent hydrophobic photolabeling of the nicotinic receptor: Electrophysiology-coordinated photochemistry and mass spectrometry

John F. Leite*†, Michael P. Blanton‡, Mona Shahgholi§, Dennis A. Dougherty§, and Henry A. Lester*

Divisions of *Biology and §Chemistry and Chemical Engineering, California Institute of Technology, Pasadena, CA 91125; and ‡Departments of Pharmacology and Anesthesiology, Texas Tech University Health Sciences Center, Lubbock, TX 79430

Edited by William A. Catterall, University of Washington School of Medicine, Seattle, WA, and approved August 22, 2003 (received for review May 16, 2003)

We characterized the differential accessibility of the nicotinic acetylcholine receptor α1 subunit in the open, closed, and desensitized states by using electrophysiology-coordinated photolabeling by several lipophilic probes followed by mass spectrometric analysis. Voltage-clamped oocytes expressing receptors were preincubated with one of the lipophilic probes and were continually exposed to acetylcholine; UV irradiation was applied during 500-ms pulses to + 40 or to −140 mV (which produced closed or ≈50% open receptors, respectively). In the open state, there was specific probe incorporation within the N-terminal domain at residues that align with the β8–β9 loop of the acetylcholine-binding protein. In the closed state, probe incorporation was identified at several sites of the N-terminal domain within the conserved cysteine loop (residues 128–142), the cytoplasmic loop (M3–M4), and M4. The labeling pattern in the M4 region is consistent with previous results, further defining the lipid-exposed face of this transmembrane α-helix. These results show regions within the N-terminal domain that are involved in gating-dependent conformational shifts, confirm that the cysteine loop resides at or near the protein-membrane interface, and show that segments of the M3–M4 loop are near to the lipid bilayer.

The nicotinic acetylcholine receptor (nAChR) is a well characterized ligand-gated ion channel in a superfamily that also includes the glycine, γ-amino-butyric acid type A, and serotonin $5HT_3$ receptors (1). Transitions among the resting (nonconducting), open (conducting), and desensitized (nonconducting) states are crucial for proper neuronal function (2). During agonist-activated channel opening, the receptor undergoes a series of molecular motions that propagate from the ligand-binding domain to the pore domain (for review see ref. 3). Given the probable complexity of these molecular motions as well as their time-dependence, it is unlikely that they will be resolved by any single methodological approach; instead, this problem requires a combination of approaches that provide both high-resolution static structural information as well as lower-resolution time- and state-dependent information.

In recent years there has been good progress toward understanding of the overall structure of the nAChR (4, 5), including high-resolution information regarding the structural changes that occur during receptor state transitions. We now have some understanding of the motions that occur during gating within the channel-lining domain (M2), and to some extent within the M1 domain (6–8). However, less is known of the transitions that occur in domains distal to the pore. Mutations at the extracellular M2–M3 loop cause congenital myasthenic syndrome by disrupting the link between ligand binding and channel activation, as revealed by effects on gating kinetics (9). The conserved cysteine loop is one structural element required for coupling ligand-binding to gating in nAChR and γ-amino-butyric acid receptor type A (10, 11). Additional recent hypotheses about conformational changes within the N-terminal region are based on the structure of the acetylcholine-binding protein (AChBP) (4, 12). Site-directed mutagenesis of nAChR, analyzed by linear free-energy relations, suggest that the transition from the resting to the open state involves a series of conformational shifts, originating at the ligand binding domain and propagating to the channel domain (13).

Hydrophobic photoreactive probes have been useful in the topological analysis of nAChR conformational states (14, 15). These probes (*i*) allow identification of protein segments that are in contact with the lipid bilayer, and (*ii*) yield inferences about secondary structure from the periodicity of photolabeled residues in a given lipid-exposed domain. Data for the hydrophobic photoreactive agent 3-trifluoromethyl-3-*m*-iodophenyl diazirine (TID) suggested a periodicity in M4 and M3 consistent with an α-helical fold. Fortuitously, TID is also a noncompetitive antagonist of the nAChR channel (16–18). Agonist-dependent changes in TID photoincorporation in the channel-lining M2 segments were observed with the nAChR, revealing the potential of using TID as a tool for studying gating-dependent conformational transitions (19). Benzophenone (BP), another hydrophobic photoreactive probe, has been used to map ligand binding sites (for review see ref. 20). This study employs the acetate and trimethyl-acetate (21) derivatives of TID (TIDBAc and TIDBTMAc, respectively) as well as BP derivatives (Fig. 1*A*).

We sought to use these probes to photolabel the open, resting, and desensitized states of the nAChR, potentially revealing state-dependent structural transitions. The sensitivity of MS encouraged us to photolabel the relatively small quantities of nAChRs present in membranes during voltage-clamp experiments. We devised a protocol that (*i*) switched from mostly closed to mostly open states within a few milliseconds, and (*ii*) photolabeled channels during a time (500 ms) too brief for appreciable changes in desensitization. We exploited the modest voltage dependence of agonist-induced nAChR channel activation: under appropriate conditions, the fraction of open channels increases at more negative potentials, at a rate of *e*-fold per 66–85 mV (22–26). In a two-electrode voltage clamping apparatus that includes a shutter-controlled UV light source (Fig. 2), irradiation was applied during either depolarizing or hyperpolarizing pulses (in the presence of ACh), thus, photolabeling channels that were mostly in the resting or open state, respectively.

Subsequently, the labeled nAChR were isolated, enzymatically digested, and analyzed by "on-line" capillary liquid chromatography (LC) with electrospray (ESI) (27) tandem mass spectrometry (MS/MS) (28) using an ion trap mass spectrometer to determine the sites of probe incorporation. In this approach, masses of photolabeled nAChR proteolytic peptides are determined by the ion trap mass spectrometer as each peptide elutes from the LC column. Potential sites of probe incorporation are subsequently determined by collision-induced dissociation (CID) (28) and MS/

This paper was submitted directly (Track II) to the PNAS office.

Abbreviations: LC, liquid chromatography; MS/MS, tandem MS; nAChR; nicotinic acetylcholine receptor; CBPP, cholesteryl benzoylphenyl propionate; BP, benzophenone; TID, 3-trifluoromethyl-3-*m*-iodophenyl diazirine; AchBP, acetylcholine-binding protein.

†To whom correspondence should be addressed. E-mail: jleite@caltech.edu.

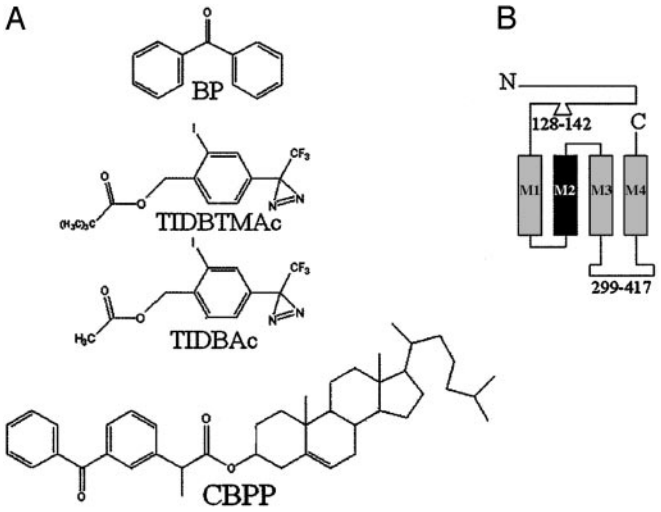

Fig. 1. Hydrophobic photoreactive probes and nAChR topology. (*A*) The structures of BP, TIDBTMAc, TIDBAc, and CBPP are illustrated. Photolabeled peptides show a mass shift of 182.1 Da, 398.1 Da, 356.1 Da, and 622.9 Da, respectively. (*B*) The commonly accepted topological model for nAChRα1. This includes the cysteine loop (residues 128–142), a four-transmembrane domain (M1–M4, residues 210–437), and a cytoplasmic loop between M3 and M4 (residues 299–417). The pore-lining domain, M2 (residues 243–261), is highlighted in black.

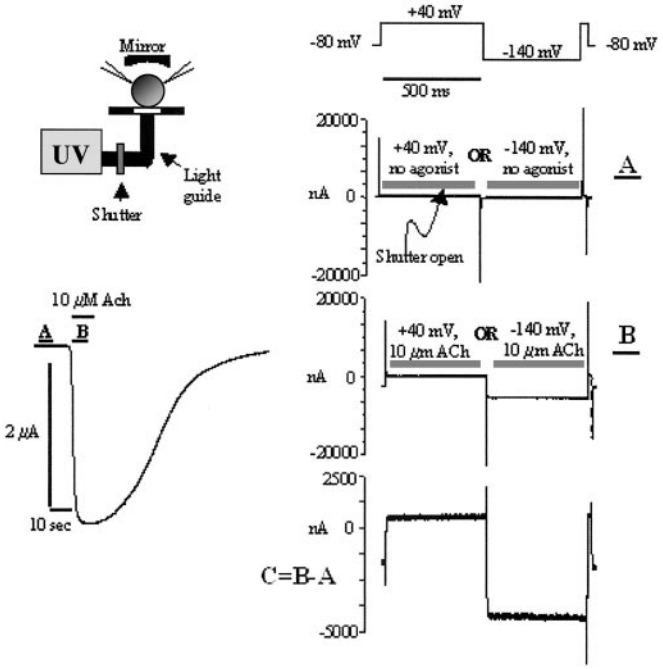

Fig. 2. Electrophysiology-coordinated photolabeling. The two-electrode voltage clamping apparatus is equipped with a UV light source. Filtered, shutter-controlled UV light (≈340 nm) irradiates the oocyte via the liquid light guide in a chamber equipped with a coverslip bottom window. The trace on the left shows the inward current induced by 10 μM ACh at a holding potential of −80 mV. The bars labeled by the letters A or B identify periods when the voltage-jump-irradiation episodes occurred, corresponding to A and B at right. The top right trace describes the voltage-jump protocol. Each sweep consisted of two successive 500-ms epochs: the membrane potential was jumped first to +40 mV, then to −140 mV. The experiments in traces A and B were conducted in the absence of ACh and the steady presence of 10 μM ACh, respectively. The ACh-induced currents are shown by subtracted traces in trace C. These sweeps were repeated five times at 1.2-s intervals, and the lamp shutter was opened either during each +40 mV epoch or during each −140 mV epoch. These experiments provided a series of oocytes described as ''+40 mV, no agonist,'' ''−140 mV, no agonist,'' ''+40 mV, ACh,'' and ''−140 mV, ACh.'' Only the oocytes described as ''−140 mV, ACh'' are expected to have appreciable number of receptors photolabeled in the open state.

MS, which can provide partial to complete amino acid sequence information. These mass spectrometric and analytic procedures are described in ref. 29.

Mass spectra of unmodified nAChR were compared with those of modified nAChR to identify those ions that had photoincorporated one or more probe moieties. MS/MS analysis of these species provided additional evidence of probe photoincorporation and often identified the specific residue where labeling had occurred. Finally, we compared data from the open state with those from the resting state and identified those residues that were uniquely labeled in the open state, and we used analogous approaches to identify residues specifically labeled in desensitized state(s). State-dependent changes were indeed identified from differences in the photolabeling patterns between the open, resting, and desensitized states. We use the acronym ECP-MS for electrophysiology-coordinated photolabeling with subsequent MS analysis.

Materials and Methods

nAChR Expression. nAChR α1, β, γ, and δ subunits (mouse muscle) were subcloned into pCDNA. A polyhistidine tag (located at the C terminus) and a hemagglutinin epitope in the M3–M4 cytoplasmic loop (after D347) were engineered into the nAChR α1 subunit (the numbering of amino acid residues after D347 is thus 8 residues greater than in the wild-type protein). Dose–response studies for this construct (mouse α1 hemagglutinin:HIS, β, γ, δ) indicated that the EC_{50} (25.5 μM) and Hill coefficient (1.26) were near previously reported values for the wild-type nAChR (6). *Xenopus laevis* (Xenopus One, Dexter, MI) oocytes were surgically removed and injected with 1 ng of total cRNA as described (6). Average currents recorded from oocytes expressing nAChR 24–48 h after injection ranged from 2 to 10 μA with 50 μM ACh.

Two-Electrode Voltage Clamping and UV Irradiation. Oocytes expressing nAChR were assayed by whole-cell recording using a two-electrode voltage clamping apparatus that includes a shutter-controlled UV light source beneath the oocyte bath (Fig. 2) (30, 31). The oocyte chamber was continuously perfused with Ca^{2+} free ND-96 at 120 chamber volumes/min for 1 min before analysis. The very high expression levels probably led to ionic accumulation and series resistance artifacts that cause underestimates of responses at −140 mV. Recordings were measured with a GeneClamp 500 (Axon Instruments) interfaced with a computer by DIGIDATA 1200 (Axon Instruments), recording and analysis performed by PCLAMP software (Axon Instruments). Oocytes were impaled with 3M KCl-filled electrodes (0.7–1.5 MΩ resistance).

Photoincorporation of Hydrophobic Photoreactive Probes. A 10 mM stock of BP (Aldrich) was prepared in 95% ethanol and stored at 4°C in a brown-glass vial. A 15 mM stock TIDBAc and a 1.5 mM stock of TIDBTMAc (21) were stored at −20°C. Cholesteryl benzoylphenyl propionate (CBPP) was synthesized by the esterification of ketoprofen (Sigma) and cholesterol (Avanti Polar Lipids) by adapting the protocol outlined in (32). Presence of the ester was confirmed by thin layer chromatography and NMR spectroscopy.

Oocytes expressing nAChR were initially preincubated (30 min) with TIDBAc, TIDBTMAc (15 μM), and BP (10 μM) in ND-96. Oocytes were transferred from the labeling solution to ND-96 medium before recording. To further remove aqueous probe, oocytes were washed on the rig with Ca^{2+}-free ND-96 for 1 min. A 1 mM solution of CBPP was mixed with 1 mM methyl-β-cyclodextrin (MCD) in ND-96. Oocytes were incubated for 40 min with the MCD:CBPP solution in the dark.

The holding potential was −80 mV; each sweep consisted of 500-ms pulses at +40 mV (500 ms), then at −140 mV (Fig. 2 *Upper*).

Table 1. nAChR α1 photolabeled residues identified by MS/MS

m/z	$(M_e-M_o)/z$	Fragment		Residue(s)	z	Probe
Open state						
721.6	0.5	153–163	-GSVVAINPE*SD*	ND	2	TIDBAc
572.2	1.2	162–172	-SDQPDL**S**NFME-	L167	3	TIDBTMAc, K^+
437.5	0.2	173–180	-*SG*EWVI*KE*-	ND	3	BP
784.4	0.2	417–441	-HILLGVFMLVCLIGTLAV**F**AGRLIE-	F435	4	TIDBTMAc, K^+
1,138.8	−1.0	417–441	-HILLGVFMLVCLIG**T**LAVFAGR*LIE*-	T431	3	TIDBAc
Closed state						
538.4	0.7	130–139	-IIVT**H**FPFDE-	H134	3	TIDBTMAc
424.5	−0.4	130–138	-IIVT**H**FPFD-	H134	3	BP
525.5	−0.3	130–139	-IIVT**H**FPFDE-	H134	3	TIDBAc
570.4	0.7	130–138	-IIVT**H**FPFD-	H134	3	CBPP
872.2	−0.6	181–200	-ARGWKHWVFYSCCPT**T**PYLD-	T196	3	BP
726.8	0.7	339–344	-**K**RIFTE-	K339	2	CBPP, K^+
995.5	1.0	417–441	-*HILL*GVFMLVCLIG*TLA*VFAGRLIE	ND	4	CBPP, K^+
871.2	0.9	417–441	-*HI*LLGVFMLV**C**LIGTLAVFAGRLIE-	C427	4	TIDBAc, NH_4^+, C
960.2	0.9	417–441	-*HI*LLGVFMLVCLIGTLAV**F**AGRLI**E**-	F435	4	TIDBAc, NH_4^+, C
955.4	0.1	417–441	-HILLGVFMLVCLIGTLAV**F**AG**R**LI**E**-	F435, R438, E441	4	TIDBAc, K^+, O
Desensitized state						
437.3	0.4	173–180	-SGE**WV**IKE-	W176, V177	3	BP
453.1	0.9	336–344	-KQEK**R**IFTE-	R340	3	BP
1,161.9	−0.1	355–380	-YAISDISGKPGPPPMGFH**S**PLIKH**P**E-	S373, P379	3	TIDBAc

Modified residues are grouped according to the macroscopic conductance state (open, closed, desensitized). Listed are the mass to charge ratios observed (m/z), the mass difference between the expected mass and the observed mass divided by the charge-state (z), $[(M_e - M_o)/z]$, the sequence of the modified proteolytic fragment (modified residues in bold, underlined type; residues in italic and underlined type indicate that a modification resides within one of those residues), and the probe used in the experiment. Salt adducts, such as potassium (K^+) or ammonium (NH_4^+), that contributed to the mass of the mass-ion are identified. Carboxyamidomethyl moieties (C) or oxidations (O) at cysteine residues are also indicated. ND, not determined.

The shutter was programmed to open either during each entire pulse +40 mV or during each entire pulse to −140 mV (Fig. 2). The shutter was opened during five successive sweeps. Photolabeling in the closed state was performed either while the oocyte was being perfused with Ca^{2+}-free ND-96, in the absence of agonist (Fig. 2, trace A) at +40 mV or at −140 mV, or during +40 mV pulses in the presence of 10 μM ACh (Fig. 2, trace B, +40 mV). These three conditions gave equivalent mass spectra and the data were pooled. Photolabeling nAChR in the open state was performed during −140-mV pulses in the presence of 10 μM ACh. To photolabel nAChR in the desensitized state, oocytes were preincubated in Ca^{2+}-free ND-96 including 500 μM Ach for 5 min, then exposed to UV irradiation for 5 s.

Extraction and Purification of nAChR α1 Subunit. Photolabeled oocytes (≈15–20 oocytes per sample) were stored at −80°C immediately after the experiment. Oocytes were thawed on ice in a 1.5-ml tube, and transferred to lysis solution [50 mM ammonium bicarbonate, pH 7.8/antiprotease (Complete, Boehringer Manheim)]. Oocytes were lysed with a 1-ml pipetter; however, yolk sacs were left intact and allowed to settle to the bottom of the tube. Total membranes were solubilized [lysis buffer, 0.1% Triton X-100 (Sigma)] and applied to 400 μl Ni^{2+} NTA agarose beads (Qiagen, Valencia, CA). After elution with solubilization buffer plus 500 mM imidazole (Aldrich), sample was dried down and resuspended in SDS/PAGE loading buffer [50 mM Tris, pH 8.0/5% 2-mercaptoethanol/1 M urea/5% glycerol/bromophenol blue (Sigma)]. Sample was loaded onto a SDS/10% PAGE gel (Bio-Rad), followed by electrophoresis for 2 h at 70 V. The nAChR α1 subunit was identified by Coomassie blue staining of the 10% gel, the gel band was excised, and the protein was extracted as described (56). The α1 subunit was digested with 1 μg of Endo-Glu-C protease (Pierce). Samples were dried and stored at −80°C until analyzed.

MS. Proteolyzed nAChR peptides were separated and analyzed by LC-MS (Finnigan model LCQ ion trap equipped with a custom nanospray interface and Surveyor LC system). Flows were adjusted for capillary chromatography by using a tee to split the flow from the HPLC unit. Uncoated fused silica PicoFrit capillary columns (inner diameter, 75 μm) (Scientific Instrument Services) were packed with 10 μm of C18 or C4 reverse-phase beads (Michrom) by using a helium bomb. Columns were packed to 5-cm length routinely yielding a backpressure of ≈1,500 psi at 500–1,000 nl/min of 10% acetonitrile, 100 mM acetic acid. Linear, dual solvent gradients were used 90% Solvent A (100 mM acetic acid)/10% Solvent B (99% acetonitrile/100 mM acetic acid) to 30% Solvent A/70% Solvent B. Spectra were acquired for 40 min; spray voltage, 2 kV; capillary temperature, 180°C; capillary voltage, 44.5 V; tube lens, 4 V.

Results and Discussion

Oocytes expressing nAChR and incubated with a hydrophobic photoreactive probe were irradiated with UV light under conditions designed to provide the largest possible voltage-dependent change in open probability (Fig. 2). In 10 μM ACh, the expected open probability at +40 mV is ≈3%; and the hyperpolarizing jump of 180 mV increased the ACh-induced conductance by nearly the expected ratio of 15.3-fold (shown by subtracted traces in Fig. 2, trace C). Although we are confident that the "closed state" receptors were a pure population, the modest voltage dependence of nAChR activation prevented us from devising a protocol that shifted nearly 100% of the channels to an open state. Therefore the "−140 mV, ACh" oocytes have a mixed population of channels, open and closed. To identify residues that were photolabeled uniquely in the open state, we emphasize residues that were labeled only in the "−140 mV, 10 μM ACh" samples (Table 1 presents this analysis).

Our procedures were designed to yield a nearly pure population of nAChR in each of three conditions: no ACh, +40 mV; no ACh, −140 mV; and 10 μM ACh, +40 mV. These experimental conditions did yield equivalent photolabeling results, and thus the data were pooled in Table 1.

Photolabeled Residues Identified Within the N-Terminal Domain. ECP-MS analysis of the nAChR α1 proteolytic fragments labeled in the open state indicated that several residues in the N-terminal domain were indeed photolabeled. The photolabeled peptides were detected at mass to charge ratios (m/z) 572.2, 721.6, and 437.5

(Table 1). Fig. 5, which is published as supporting information on the PNAS web site, www.pnas.org, shows a typical tandem mass spectrum of one of these photolabeled peptides, in this case, the ion with m/z 721.6 ($[M + 2H^+]^{2+}$), which corresponds to G153–D163 plus one TIDBAc modification. The photolabeled y ion series detected suggests that either y_1 or y_2 is the site of TIDBAc incorporation. The y_3 ion, because of the presence of proline, is the most abundant fragment ion in the mass spectrum (see ref. 33 for MS/MS nomenclature). Other prominent ions in this mass spectrum are m/z 446.4 and 359.2, which are attributed to unlabeled y_4 and protonated TIDBAc. It appears that y_4 loses the TIDBAc label during collision-induced dissociation. Examination of this MS/MS mass spectrum narrows the site of TIDBAc incorporation to the carboxy end of the peptide, residues S162 or D163. Similarly, MS/MS analysis of photolabeled peptide of m/z 437.5 narrowed the site of probe (BP) incorporation to S173/G174 and K179/E180. For the photolabeled peptide with m/z 572.2, MS/MS analysis indicated that L167 was uniquely labeled with TIDBTMAc. Thus, unique nAChRα1 residues were found photolabeled in the open state between residues S162 and E180.

Analysis of nAChR α1 photolabeled in the resting state also identified labeled residues located in the N-terminal domain. In this case, H134 was photolabeled with TIDBTMAc (Fig. 6, which is published as supporting information on the PNAS web site) as well as with TIDBAc and BP (Table 1). Interestingly, this residue is located within the highly conserved cysteine loop (see Fig. 1*B*), found within the soluble N-terminal domain and thus was not expected to gain access to the membrane interior. To confirm that labeling of H134 was occurring at the protein-membrane interface, we synthesized CBPP (Fig. 1*A*), and used it to photolabel nAChR α1. Previous studies have mapped the cholesterol-binding site of nAChR within the transmembrane domain (34, 35), specifically within M1 and M4 (36). Thus, we expected CBPP to partition into the annulus of phospholipid and native cholesterol around the nAChR. As anticipated, photolabeling of M4 was observed (Table 1, discussed further below) suggesting that CBPP localizes similarly to cholesterol and cholesterol analogs. CBPP-photolabeled H134 was detected in the proteolytic fragment I130-D138 at m/z 570.4, $[M+3H^+]^{3+}$. MS/MS analysis of this peptide confirmed that H134 was photolabeled by CBPP (Table 1). Another residue photolabeled in the resting state was T196. This residue was found in the proteolytic fragment -ARGWKHWVFYSCCPTTPYLD-, which was detected at m/z 872.2 as a singly BP-photolabeled peptide (Table 1). However, photolabeling at this site was never observed by using the larger probes (i.e., TID derivatives or CBPP). We hypothesize that BP may have partitioned into a hydrophobic pocket that remains inaccessible to other probes.

Photolabeling of nAChR α1 residues located in the N-terminal domain was also observed in the desensitized state. Specifically, residues W176 and V177 (m/z 437.3) were modified by BP (Table 1). These residues lie in close proximity to residues identified as photolabeled by BP in the open state, S173/G174 and K179/E180 (see above). Although photolabeling at W176 and V177 is uniquely observed in the desensitized state, we cannot assess whether this new photolabeling pattern arises (*i*) from a conformational shift occurring in the region within residues 173–180, or (*ii*) from changes in structure(s) surrounding 173–180.

The nAChR N-terminal domain shares key residues with AChBP of *Lymnaea stagnalis* (37), whose crystal structure (12) may thus serve as a high-resolution model for the N-terminal domain of the nAChR. We have projected our photolabeling data onto the AChBP structure (Fig. 3): highlighted AChBP residues align with photolabeled nAChR α1residues. In the open state (Fig. 3*A*), modifications occurred within the region between residues S162 and E180. This region aligns with the AChBP β8–β9 loop (12). Thus, our results suggest that this region of the nAChR α1 N-terminal domain undergo conformational changes during the transition from the resting state to the open state. This finding is consistent with a recent report that compares the AChBP structure with cryoelectron microscopy imaging of *Torpedo* nAChR in the resting and open state, suggesting that the α subunit outer sheets (which include β8–β9) rotate slightly as well as tilt during the resting to open state transition (4). Also, our results are consistent with fluorescence studies that suggest that a monoclonal antibody directed at the high-affinity agonist binding site can induce the movement of the low-affinity site toward the membrane (38) as well as studies of γ-amino-butyric acid receptor type A that suggest the β8–β9 loop changes its solvent exposure during channel gating (39).

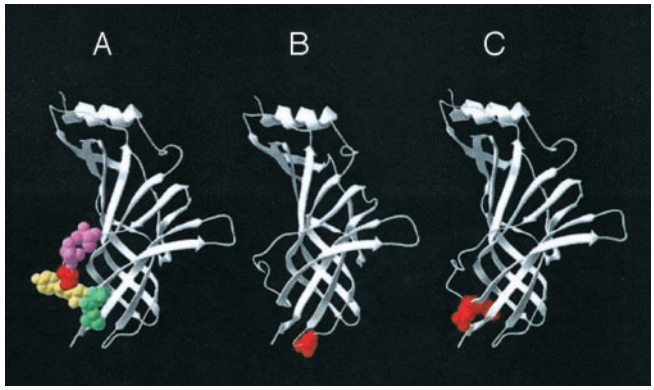

Fig. 3. AChBP residues homologous to nAChRα1 photolabeled residues highlighted within the AChBP monomer structure. (*A*) AChBP residues photolabeled in the open state. AChBP residues T156, N158, S162, Y168, S169, L174, and D175 align with nAChRα1 residues S162, D163, L167, S173, G174, K179, and E180, respectively. In the open state, photolabeling is present at L167 (red), residues S162 or D163 (purple), S173 or G174 (yellow), and K179 or E180 (green). (*B*) The AChBP D129 side chain (red), which aligns with the nAChRα1 H134, photolabeled in the closed state. (*C*) AChBP residues F171 and K172 which correspond to nAChRα1 residues W176 and V177, respectively. These residues (red) were identified as photolabeled in the desensitized state.

Fig. 3*B* illustrates a single subunit of AChBP with the side chain of D129 highlighted (which aligns with nAChR α1 H134). This residue lies at the very bottom of the structure and, in the N-terminal domain, would lie close to the membrane surface. Furthermore, the cysteine loop in nAChR subunits contains more hydrophobic residues than in AChBP (12). Therefore, we conclude that this conserved structure makes contact with the membrane surface in the resting state, and gains access to hydrophobic photoreactive probes.

Fig. 3*C* highlights AChBP residues F171 and E172, which align with nAChR α1 residues W176 and V177 (12). These residues reside at the bottom of the AChBP structure. Correspondingly, we conclude that nAChR α1 W176 and V177 move close to the membrane surface in the desensitized state.

We have identified photolabeling in the N-terminal domain in the open, resting, and desensitized states. For the most part, we believe that this differential state-dependent labeling shows residues that approach the membrane. However, it is possible that residues are photolabeled when they contact a hydrophobic pocket (either within the N-terminal domain or at the transmembrane domain) and that a photoreactive probe may partition to this region, rather than make contact with the membrane surface. Indeed, this appears likely for the specific case of T196, photolabeled in the resting state uniquely by the compact BP molecule, but not detectably by TID or CBPP. The reactivity of different probes varies among amino acid side chains (40), so that in the present study some residues may escape labeling primarily of their low reactivity. We did not study possible labeling at the β8–β9 loop in the open state by CBPP because CBPP may alter nAChR function in the open state (41, 42).

Photolabeled Residues Identified Within the M3–M4 Loop. K339 (m/z 726.8) is an example of a residue identified as photolabeled by CBPP under both depolarizing and hyperpolarizing conditions (Table 1). Topology models place this residue in an intracellular loop (Fig. 1*B*) (3). As noted above, it is not possible to shift the entire nAChR population to the open state during the hyperpolarizing pulse. Thus, one expects to observe a residue photolabeled under both experimental conditions even if the residue is accessible to photoprobes in only the resting state; however, our data do not indicate whether this labeling occurred uniquely in the open state conformation.

In desensitized nAChRs, unique photolabeled residues were identified in the M3–M4 loop. For example, photolabeling by BP was detected at residue R340 (m/z 453.1), which is immediately adjacent to the K339 residue that was photolabeled by CBPP in the resting state (m/z 726.8). Although photolabeling of this residue is unique to the desensitized state, we cannot assess whether this shift in the labeling profile is significant, given the close proximity of the two modified residues. Furthermore, both K339 and R340 are located in close proximity to the engineered hemagglutinin epitope (residues 348–355), which may perturb the native structure within this region in a fashion that is not detectable by the dose-response analysis. Residues S373 and P379 within the α1 M3–M4 cytoplasmic loop (m/z 1161.9) were also uniquely photolabeled in the desensitized state. Photolabeled residues identified by the present study suggest that segments of the M3–M4 loop may come in contact with the membrane surface and may undergo conformational shifts during the transition from the resting state to the desensitized state. These results are consistent with limited proteolysis studies of the glycine receptor that suggest regions of the M3–M4 loop are peripherally associated with the membrane surface via either electrostatic interactions with phospholipids head groups or residue side chains from transmembrane domains (43). These results are also consistent with imaging studies (44) and mutagenesis studies (45), suggesting that the M3–M4 loop, in association with the pore, is part of the ion conduction pathway.

Photolabeled Residues Identified Within M4. Previous studies reveal that TID photoincorporates into each of the four membrane spanning segments (Fig. 1*B*); labeling of the M1, M3, and M4 segments is consistent with direct exposure to the lipid bilayer (reviewed in ref. 18). In the present study, we were able to detect several residues within the nAChR α1 M4 segment that were photolabeled with TID analogs (Table 1) in the resting state. Specifically, nAChR α1 C427 (Fig. 7, which is published as supporting information on the PNAS web site), F435, R438, and E441 were identified by MS/MS analysis as photolabeled by a TIDBAc moiety (Table 1).

In the open state, we identified T431 as photolabeled by TIDBTMAc, in addition to TID-modified residues that were identified in the resting state. Although T431 is a uniquely photolabeled residue in the open state, this residue lies on the same face of the α-helical projection of M4 (Fig. 4) as the other photolabeled residues from the resting state. Thus, we cannot assess whether M4 undergoes any conformational shift during the transition from the resting state to the open state by using the methodology presented in this report.

The results shown in Fig. 4 illustrate that M4 photolabeled residues identified by this study reside on the same helical face as residues identified in previously published reports. Thus the present results further define the lipid-exposed face of the M4 transmembrane α-helix (46, 47).

Desensitization Does Not Distort the Identification of Residues Labeled in the Open State. Desensitization is a complication. At nicotinic receptors, desensitization is a shorthand word for a complex and incompletely described set of agonist-induced transitions to closed states. We assessed a slower phase of desensitization by noting the currents induced by 10 μM ACh at the -80 mV holding potential during the photolabeling experiments (for instance, Fig. 2 *Left*). The data showed that current declined by no more than 1% by the end of the 6-s period that comprised the set of voltage-clamp pulses. However, an additional possible source of desensitized receptors is fast-onset desensitization, which occurs at time constants on the order of 100–300 ms at mouse muscle nicotinic receptors at the ACh concentrations we have used (48). As usual in nAChR experiments, fast-onset desensitization might actually occur during the solution change ($\approx$500 ms). Both experimental conditions "-140 mV, ACh" and "$+40$ mV, ACh" involve exposure to the same agonist concentration for the same length of time, and our procedure eliminated photolabeled residues common to both experimental conditions. Importantly, we found no time-dependent changes in ACh-induced current during the sojourns at $+40$ mV or at -140 mV (Fig. 2*C*). Therefore, fast-onset desensitization may not be voltage dependent; but in any case, we conclude that desensitization did not change between the $+40$ mV and -140 mV pulses. Therefore, the additional residues labeled in "-140 mV, ACh" oocytes cannot be distorted by fast-onset desensitization.

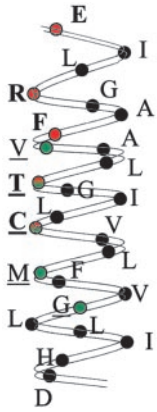

Fig. 4. Helical projection of nAChRα1 M4 residues. Residues accessible to TID analogs identified in the closed and open states are shown in red circles with bold type. For further comparison, shown in green circles with underlined type are the residues in the mouse muscle α1 AChR subunit that align with those in *Torpedo* nAChR α-subunit previously photolabeled by TID (46, 47, 55). C427 and T431 (shown in bold underlined type with red/green circles) were identified by TID incorporation both in previous studies and in the present study.

MS for Analyzing Ion Channel Conformational States. MS provides a powerful and sensitive approach for analyzing chemically modified residues in membrane proteins (49, 50). ECP extends this technique for analyzing short-lived conformational states. The present approach does not require the use of site-directed mutants, and so the potential structural perturbations induced by amino acid substitution are avoided. Furthermore, the present procedure does not rely on a change in electrophysiological function to determine whether reaction with a specific site has occurred. Thus, we are able to analyze regions that might be functionally "silent" upon reaction with a chemical reagent. Presently, there are limitations to the technique: we were unable to detect the M1–M3 transmembrane segments. We hypothesize that the hydrophobic and aggregative nature of this region not only prevents efficient enzymatic proteolysis within this region, but possibly limits efficient ionization of proteolytic fragments during MS analysis. However, the nAChR α1 M4 segment was detected and indeed, photolabeled residues were identified by MS/MS analysis (Table 1). Optimized solubilization, proteolysis, and analysis techniques may allow detection of other transmembrane segments.

Table 1 lists mass accuracies of the detected photolabeled peptides. Some photolabeled peptides deviated markedly from

expected masses. These deviations cannot be explained by ion statistics, inability to effectively isolate the monoisotopic fragments, fluctuation in radio frequency isolation of an ion, or mass shift stemming from dissociative collisions between analyte ions and buffer gas (51–53). Instead, we have determined, by analyzing synthetic BP-photolabeled peptides, that the BP moiety underwent a phenyl rearrangement and ketone formation, losing two hydrogen atoms and producing species that were 2 Da lower in mass than predicted (54). The data in Table 1 have not been adjusted to account for effects of probe chemistry; however, these effects do not alter the identity of the photolabeled residues.

In mass spectrometric studies of membrane proteins, as in studies on other proteins, the extent of labeling can be measured by comparing modified and unmodified peaks (50). During the LC-MS analyses, unmodified proteolytic fragments often coeluted with or just before the analogous modified proteolytic fragments. We therefore estimated labeling efficiency for a specific peptide by calculating the ratio (peak $\text{area}_{\text{photolabeled peptide}}$)/(peak $\text{area}_{\text{photolabeled peptide}}$ + peak $\text{area}_{\text{unlabeled peptide}}$). These estimates assume that the photolabeled peptides show the same ionization efficiency as the analogous unlabeled peptides, and that the photolabel is not affecting the efficiency of proteolytic cleavages at neighboring sites. Should photolabeling interfere with proteolytic cleavage at neighboring residues or affect the ionization of the proteolytic fragment, it is likely to decrease the observed abundance of the photolabeled peptides and therefore underestimate the actual photolabeling efficiency. In this fashion, we estimate that labeling efficiency for the I130-E139 region is ≈65% for TIDBAc and 47% for CBPP labeling within I130-D138. In a separate study, we photolabeled a synthetic peptide corresponding to nAChR α1 residues 130–139 with BP *in vitro* and observed ≈10% labeling yields. Yields from the present study are markedly higher than those reported for TID labeling in *Torpedo* membranes (1%; ref. 17). The reason for this difference may be the high receptor density of *Torpedo* electroplaque membranes, which might interfere with probe access to the receptor. We identified several M4 proteolytic fragments that included more than one photoincorporation, fully consistent with the high probability that we determined for individual photoincorporations. These estimates, combined with reproducibility of labeling sites, indicate that a significant and representative population of receptors is being photolabeled.

Summary. We used electrophysiology-coordinated hydrophobic photochemical labeling of the nAChR coupled to MS analysis to identify residues in the α1 subunit that are uniquely photolabeled in each of three functional states. Interestingly, we have detected photolabeling of α H134 in the conserved cysteine loop in the resting state. Also, we have identified several residues photolabeled in the open state, located in a region that corresponds to the AChBP β8–β9 loop. These results suggest that, during the transition from the resting state to the open state, the β8–β9 loop structure moves from a hydrophilic environment to a hydrophobic environment, and possibly makes contact with the membrane surface. Furthermore, several photolabeled residues within the M3–M4 loop have been identified in the resting state and desensitized state. These results suggest that regions of the M3–M4 loop come in contact with the membrane surface and also may shift conformation during the transition from the resting state to the desensitized state.

1. Ortells, M. O. & Lunt, G. G. (1995) *Trends Neurosci.* **18,** 121–127.
2. Engel, A. G., Ohno, K. & Sine, S. M. (2002) *Mol. Neurobiol.* **26,** 347–367.
3. Karlin, A. (2002) *Nat. Rev. Neurosci.* **3,** 102–114.
4. Unwin, N., Miyazawa, A., Li, J. & Fujiyoshi, Y. (2002) *J. Mol. Biol.* **319,** 1165–1176.
5. Miyazawa, A., Fujiyoshi, Y. & Unwin, N. (2003) *Nature* **424,** 949–955.
6. England, P. M., Zhang, Y., Dougherty, D. A. & Lester, H. A. (1999) *Cell* **96,** 89–98.
7. Unwin, N. (1995) *Nature* **373,** 37–43.
8. Wilson, G. & Karlin, A. (2001) *Proc. Natl. Acad. Sci. USA* **98,** 1241–1248.
9. Grosman, C., Salamone, F. N., Sine, S. M. & Auerbach, A. (2000) *J. Gen. Physiol.* **116,** 327–339.
10. Shen, X. M., Ohno, K., Tsujino, A., Brengman, J. M., Gingold, M., Sine, S. M. & Engel, A. G. (2003) *J. Clin. Invest.* **111,** 497–505.
11. Kash, T. L., Jenkins, A., Kelley, J. C., Trudell, J. R. & Harrison, N. L. (2003) *Nature* **421,** 272–275.
12. Brejc, K., van Dijk, W. J., Klaassen, R. V., Schuurmans, M., van Der Oost, J., Smit, A. B. & Sixma, T. K. (2001) *Nature* **411,** 269–276.
13. Grosman, C., Zhou, M. & Auerbach, A. (2000) *Nature* **403,** 773–776.
14. Heidmann, T. & Changeux, J. P. (1986) *Biochemistry* **25,** 6109–6113.
15. DiPaola, M., Kao, P. N. & Karlin, A. (1990) *J. Biol. Chem.* **265,** 11017–11029.
16. White, B. H., Howard, S., Cohen, S. G. & Cohen, J. B. (1991) *J. Biol. Chem.* **266,** 21595–21607.
17. White, B. H. & Cohen, J. B. (1992) *J. Biol. Chem.* **267,** 15770–15783.
18. Arias, H. R. (1998) *Biochim. Biophys. Acta* **1376,** 173–220.
19. Chiara, D. C., Kloczewiak, M. A., Addona, G. H., Yu, J. A., Cohen, J. B. & Miller, K. W. (2001) *Biochemistry* **40,** 296–304.
20. Dorman, G. & Prestwich, G. D. (1994) *Biochemistry* **33,** 5661–5673.
21. Blanton, M. P., McCardy, E. A. & Gallagher, M. J. (2000) *J. Biol. Chem.* **275,** 3469–3478.
22. Magleby, K. L. & Stevens, C. F. (1972) *J. Physiol.* **223,** 151–171.
23. Neher, E. & Sakmann, B. (1975) *Proc. Nat. Acad. Sci. USA* **72,** 2140–2144.
24. Sheridan, R. E. & Lester, H. A. (1975) *Proc. Natl. Acad. Sci. USA* **72,** 3496–3500.
25. Auerbach, A., Sigurdson, W., Chen, J. & Akk, G. (1996) *J. Physiol. (London)* **494,** 155–170.
26. Lester, H. A., Koblin, D. D. & Sheridan, R. E. (1978) *Biophys. J.* **21,** 181–194.
27. Fenn, J. B., Mann, M., Meng, C. K., Wong, S. F. & Whitehouse, C. M. (1989) *Science* **246,** 64–71.
28. Hunt, D. F., Yates, J. R., Shebanowitz, J., Winston, S. & Hauer, C. R. (1986) *Proc. Natl. Acad. Sci. USA* **83,** 6233–6237.
29. Kinter, M. & Nicholas, S. (2000) *Protein Sequencing and Identification Using Tandem Mass Spectrometry* (Wiley, New York).
30. Miller, J. C., Silverman, S. K., England, P. M., Dougherty, D. A. & Lester, H. A. (1998) *Neuron* **20,** 619–624.
31. Tong, Y., Brandt, G. S., Li, M., Shapovalov, G., Slimko, E., Karschin, A., Dougherty, D. A. & Lester, H. A. (2001) *J. Gen. Physiol.* **117,** 103–118.
32. Bujanowski, V. J., Katsoulis, D. E. & Ziemelis, M. J. (1994) *J. Math. Chem.* **4,** 1181–1187.
33. Roepstorff, P. & Fohlman, J. (1984) *Biomed. Mass Spectrom.* **11,** 601.
34. Addona, G. H., Sandermann, H., Jr., Kloczewiak, M. A., Husain, S. S. & Miller, K. W. (1998) *Biochim. Biophys. Acta* **1370,** 299–309.
35. Narayanaswami, V. & McNamee, M. G. (1993) *Biochemistry* **32,** 12420–12427.
36. Corbin, J., Wang, H. H. & Blanton, M. P. (1998) *Biochim. Biophys. Acta* **1414,** 65–74.
37. Smit, A. B., Syed, N. I., Schaap, D., van Minnen, J., Klumperman, J., Kits, K. S., Lodder, H., van der Schors, R. C., van Elk, R., Sorgedrager, B., *et al.* (2001) *Nature* **411,** 252–255.
38. Valenzuela, C. F., Dowding, A. J., Arias, H. R. & Johnson, D. A. (1994) *Biochemistry* **33,** 6586–6594.
39. Newell, J. G. & Czajkowski, C. (2003) *J. Biol. Chem.* **278,** 13166–13172.
40. Deseke, E., Nakatani, Y. & Ourisson, G. (1998) *Eur. J. Org. Chem.* **2,** 243–251.
41. Rankin, S. E., Addona, G. H., Kloczewiak, M. A., Bugge, B. & Miller, K. W. (1997) *Biophys. J.* **73,** 2446–2455.
42. Santiago, J., Guzman, G. R., Rojas, L. V., Marti, R., Asmar-Rovira, G. A., Santana, L. F., McNamee, M. & Lasalde-Dominicci, J. A. (2001) *J. Biol. Chem.* **276,** 46523–46532.
43. Leite, J. F., Amoscato, A. & Cascio, M. (2000) *J. Biol. Chem.* **275,** 13683–13689.
44. Miyazawa, A., Fujiyoshi, Y., Stowell, M. & Unwin, N. (1999) *J. Mol. Biol.* **288,** 765–786.
45. Valor, L. M., Mulet, J., Sala, F., Sala, S., Ballesta, J. J. & Criado, M. (2002) *Biochemistry* **41,** 7931–7938.
46. Blanton, M. P. & Cohen, J. B. (1992) *Biochemistry* **31,** 3738–3750.
47. Blanton, M. P. & Cohen, J. B. (1994) *Biochemistry* **33,** 2859–2872.
48. Dilger, J. P. & Liu, Y. (1992) *Pflugers Arch.* **420,** 479–485.
49. Leite, J. F. & Cascio, M. (2002) *Biochemistry* **41,** 6140–6148.
50. Weinglass, A. B., Whitelegge, J. P., Hu, Y., Verner, G. E., Faull, K. F. & Kaback, H. R. (2003) *EMBO J.* **22,** 1467–1477.
51. Murphy, J. P., III, & Yost, R. A. (2000) *Rapid Commun. Mass Spectrom.* **14,** 270–273.
52. Vachet, R. W., Hartman, J. A. R. & Callahan, J. H. (1998) *J. Mass Spectrom.* **33,** 1209–1225.
53. Peng, Y., Plass, W. R. & Cooks, R. G. (2002) *J. Am. Soc. Mass Spectrom.* **13,** 623–629.
54. Leite, J. F., Dougherty, D. A., Lester, H. A. & Shahgholi, M. (2003) *Rapid Commun. Mass Spectrom.* **17,** 1677–1684.
55. Blanton, M. P., McCardy, E. A., Huggins, A. & Parikh, D. (1998) *Biochemistry* **37,** 14545–14555.
56. Zhou, J., Rusnak, F., Colonius, T. & Hathaway, G. M. (2000) *Rapid Commun. Mass Spectrom*. **14,** 432–438.